THE JOURNAL OF PHYSICAL CHEMISTRY

Freie Universität Berlin

Subscriber access provided by UB + Fachbibliothek Chemie | (FU-Bibliothekssystem)

Article

Understanding Aggregation Induced Emission in Molecular Crystals: Insights from Theory

Davide Presti, Liam Wilbraham, Cecilia Targa, Frédéric Labat, Alfonso Pedone, Maria Cristina Menziani, Ilaria Ciofini, and Carlo Adamo

J. Phys. Chem. C, **Just Accepted Manuscript** • DOI: 10.1021/acs.jpcc.7b00488 • Publication Date (Web): 27 Feb 2017

ACS Publications

The Journal of Physical Chemistry C is published by the American Chemical Society. 1155 Sixteenth Street N.W., Washington, DC 20036

Understanding Aggregation Induced Emission in Molecular Crystals: Insights from Theory

Davide Presti[1,¶], Liam Wilbraham[2,¶], Cecilia Targa,[1] Frédéric Labat[2], Alfonso Pedone[1] , Maria Cristina Menziani[1], Ilaria Ciofini[2] and Carlo Adamo[*2]

[1] *Dipartimento di Scienze Chimiche e Geologiche, Università di Modena e Reggio-Emilia, 183 via G. Campi, I-41125 Modena, Italy.*

[2] *PSL Research University, Institut de Recherche de Chimie Paris IRCP, CNRS−Chimie ParisTech, 11 rue P. et M. Curie, F-75005 Paris 05, France.*

Abstract

Aggregation-induced emission can often be explained via the restriction of intramolecular rotation paradigm and/or excimer formation. The enhanced luminescence recently observed for aggregates of Fluorenone derivatives are no exception. In this work, however, we use a recently developed excited state electrostatic embedding technique to demonstrate that enhanced emission in diphenylfluorenone can be rationalized by considering a single-molecule process, in which the field induced by the crystalline environment at the excited state enhances the relative brightness of otherwise poorly emissive states, resulting in both enhanced fluorescence and a substantial bathochromic shift when compared with emission in dilute solution.

¶ DP and LW contributed equally to this work. *Corresponding Authors: carlo.adamo@chimie-paristech.fr

1. Introduction

In most cases, the bright fluorescence observed in chromophores in dilute solutions is absent upon the aggregation or precipitation of the same chromophore, where self-quenching triggered by intermolecular interactions such as π-π stacking renders the system non-fluorescent.[1] This aggregation-caused-quenching (ACQ) poses a substantial challenge to the design and development of solid-state light-emitting devices for applications such as biological and chemical sensing and organic light-emitting diodes.[2–6] A phenomenon which can be described as the mirror-image of this effect can, however, be observed in a special class of materials that exhibit weak or no fluorescence in dilute solution, yet demonstrate strong fluorescence in the solid-state. This is known as aggregation induced emission (AIE),[7] and is generally observed in chromophores comprising rigid moieties, which are capable of rotation relative to a relatively inflexible core.[8] AIE is facilitated by the steric interactions introduced in the solid-state which reduce the rotational flexibility of the rotator moieties (the so-called Restriction of Intramolecular Rotation, RIR) and subsequently block potentially fast deactivation pathways otherwise fully accessible in dilute solution.[7,9–12]

From a theoretical point of view, attempts have been made to rationalize this process via the calculation of potential energy surfaces along rotational trajectories and the analysis of the non-radiative decay rates along these pathways.[13,14] While this concept can readily explain AIE observed in chromophores such as trimethylsilole,[15] in which the emission of the aggregate is of a similar wavelength to that of the molecule in solution, it is not sufficient to explain large solvatochromic-like effects observed in some AIE chromophores.

The concomitant brightening and significant bathochromic shift of emission band maxima during the aggregation of such chromophores is usually attributed to the formation of excimers. This is

experimentally substantiated by an apparent broadening of the emission band itself, along with an increased excited state lifetime observed via time resolved fluorescence techniques.[16]

2,7-diphenylfluorenone (DPF) is one such chromophore, demonstrating more than a 150 nm red shift of the emission band after aggregation, which is attributed to excited state excimer formation.[16–18] This work will demonstrate, however, that AIE in DPF arises from a single-molecule process rather than the formation of excimers. Using a recently developed excited state electrostatic embedding model as an approximation of the solid state environment,[19] it will be shown that the field induced by the crystalline environment can enhance the relative brightness of otherwise poorly emissive states in DPF, resulting in both enhanced fluorescence and a substantial bathochromic shift when compared with emission in dilute solution.

2. Computational Details

Single molecule calculations. DFT and TDDFT calculations have been used to investigate the ground and excited state properties of a single DPF molecule in vacuum and in THF solution.

The latter were described by using the Conductor-like Polarizable continuum solvation Model (C-PCM) in the linear response formulation.[20]

Ground and excited state geometry optimizations and absorption/emission energies have been performed using both B3LYP[21,22] and CAM-B3LYP[23] functionals coupled with the 6-31+G(d,p) basis set which represents the best compromise between cost and quality of the geometrical parameters (see table S.2 of SI). All these calculations have been carried out with the Gaussian09 suite of programs.[24]

Periodic Solid state calculations. In order to determine the equilibrium atomic positions and unit cell parameters for subsequent embedding techniques, ground-state calculations have been carried out on bulk DPF, employing the parallel version of the CRYSTAL09 package.[25,26] With

the purpose of obtaining an electronic ground-state structurally as close as possible to the experimental one, we performed a dispersion-corrected B3LYP-D*[27]/6-31G(d,p) full optimization (cell and atomic positions) of the solid crystalline system, shown in **Figure S.3** of the Supporting Information (SI) (168 atoms/cell, *C*mc2$_1$, *Z*=4). In such a case, diffuse functions were not utilized to avoid basis-set linear dependence issues. The Monkhorst-Pack grid was set to 6 *k*-points within the Irreducible Brillouin Zone. An extra-large DFT grid (75 radial and 974 angular points) was chosen. The tolerances on Coulomb and exchange bielectronic integrals were set to 10^{-9}, 10^{-9}, 10^{-9}, 10^{-9}, 10^{-18} a.u.

In order to determine excited state properties of crystalline DPF, the QM/QM' ONIOM and the Self-Consistent Ewald embedding methods have been used.

ONIOM QM/QM' calculations. In this approach a sufficiently large cluster is cut from a crystal supercell and treated at the QM/QM' level in which the high level region consists of the central single DPF molecule or a central dimer as shown in Figure 1a and S.4 of ESI, respectively.

The low-level region includes 20 DPF molecules for the monomer model (**Figure 1a**), whereas it includes 20 and 22 DPF molecules (the nearest-neighbors molecules, within a range of 3.8-4.0 Å) for the two dimer models considered, **Dimer 1** and **Dimer 2**, respectively (see SI, **Figure S.4**).

Monomer and dimer vertical absorption energies have been computed at the TD-DFT/6-31+G(d,p):HF/STO-3G level of theory, at the optimized crystalline geometry (*vide supra*) whereas the emission spectra were computed by optimizing at the same level of theory the (lowest) bright excited singlets (S_1 and S_3 states) involved in the fluorescent emission observed experimentally. The S_2 state was not considered since, in every case, it was computed to be nearly/totally a *dark* state (oscillator strength f=0.000 a.u.) (see **Table S5**). As DFT approximations, B3LYP and CAM-B3LYP functionals were considered for the high-level QM region. Following previous investigations[28–30] the low level region was treated at the Hartree-

Fock (HF) level coupled with the Slater-type STO-3G minimal basis set since it provides Mulliken charges similar to that obtained with more accurate calculations.

Self-Consistent Ewald embedding calculations. The solid state environment has also been modelled using the so-called Self-Consistent Ewald approach (SC-Ewald), previously developed by some of us.[19] Briefly, this process seeks to approximate the excited state crystalline environment via a large array of point charges while, at the same time, performing a charge fitting process to reproduce the infinite electrostatic potential of the fully periodic system, using the approach first developed by Derenzo and co-workers.[31]

The charge array was composed of a 5×5×5 supercell, in order to obtain a cube-like distribution of point charges, giving a total of approximately 11000 point charges. For the charge fitting procedure, the fixed charge zone (Zone 2, see **Figure 1b**) was set to an origin-centered sphere containing 1500 atoms in order to ensure the QM region (Zone 1) is not close to the 'outside wall' of Zone 2. The resulting fitted charges in Zone 3 produced an adequate root mean square (RMS) error of the Ewald potential within Zone 1 of less than 0.1 μV.

To model the crystalline environment at the excited state, this charge array was recomputed self-consistently using the Mulliken charges derived from the electronic density of the excited state of interest (S_1 and S_3 states in this case), applying a convergence criterion of 0.001 |e-| with respect to the mean average deviation of the computed charges in Zone 1. In order to avoid numerical instabilities,[32] the SC-Ewald procedure was carried out using a reduced basis set (6-31G), before reverting to the full basis set (6-31+G(d,p)) for the calculation of optical absorption and emission properties within the generated charge background.

3. Results and Discussion

Following the experimental interpretation of excimer formation as the root cause of AIE in DPF, absorption features were first determined for two sets of dimers found in crystalline DPF. From

Figure 2, it can be clearly observed that, regardless of the dimer chosen, the effect on the calculated absorption spectrum - with respect to that of the monomer - is negligible. This observation also holds when the solid state environment is approximated using the ONIOM method. Together, these results show that, at least in the vertical absorption regime, the intermolecular coupling is not sufficient to alter the observed photophysical properties either in terms of energy or absorption intensity. From these results, it is then necessary to consider alternative mechanisms to rationalize the AIE behaviour of DPF. In the following, starting from a monomer picture, it will be shown that both the absorption and emission spectra of aggregated DPF can be explained via a single-molecule process, facilitated by interactions with the crystalline environment at the excited state.

Figure 3 shows the UV-Visible absorption spectra computed at B3LYP and CAM-B3LYP level for the DPF monomer in vacuum, THF (implicit) solution and with the ONIOM QM/QM' and SC-Ewald embedding protocols.

At first glance, a qualitative accuracy of both functionals for the overall spectral band shapes can be observed, with respect to the experimental counterpart in concentrated (60 μM) THF solution (Figure 1g of the experimental paper[16]) – where DPF is supposed to be emissive due to being in an aggregated form. Also, an almost quantitative spectral characterization is provided by B3LYP in terms of λ_{max} wavelengths, relative band intensities and band shapes. It should be noted that in the following, absorption spectra will be compared with those in concentrated THF solution (60 μM), whereas λ_{max} refer to those available, i.e. obtained in THF/water (20 μM) which provide, nonetheless, the same optical transitions.

In more detail, the main transitions found experimentally (Table 1 of Ref.[16]) – corresponding to 4.34 eV, 3.64 eV and 2.63 eV (286 nm, 341 nm, and 471 nm) – are quite well reproduced. A sizable bathochromic (hypsochromic) shift is observed with B3LYP (CAM-B3LYP) for the high

energy/most intense π-π* transition located experimentally at 4.34 eV which is, however, of little interest for potential AIE mechanisms, due to the very low probability of populating the associated singlet excited state ($S_5 \leftarrow S_0$).

Moving towards lower energy transitions, a better description is given by B3LYP for the two convoluted bands at ca. 3.84 eV ($S_3 \leftarrow S_0$ and $S_2 \leftarrow S_0$ transitions with π-π* character), whereas CAM-B3LYP predicts hypsochromically shifted transitions. It is worth noting here that the vibronic band shape observed in the experimental spectrum is not accounted for within the current computational protocol.[33–37]

A broad and weak absorption band at ca. 2.63 eV (471 nm, not indicated in the experimental work for the 20 μM THF solution, but nonetheless producing a distinguishable non-zero absorption signal, see Figure 1c of Ref.[16]) arises in the computed B3LYP spectra, and it is consistent with the weak absorption of the first (HOMO-LUMO, $S_1 \leftarrow S_0$) transition, possessing CT character. Here, the electronic effects from the use of different structural and environmental descriptions of DPF highlight that: i) as expected, B3LYP gives, in general, a better prediction of the $S_1 \leftarrow S_0$ wavelength, compared to experiment, but this could be due to the limited through-space character of this transition, whereas ii) CAM-B3LYP, though sizably underestimating the λ_{max} of all transitions, it gives a more homogeneous and systematic shift by using the different models. Moreover, recalling that such functional is known to perform well in describing transitions with a CT character,[23,38] we expect it to provide reasonable values for vertical emission with respect to B3LYP, which usually predicts overestimated transitions. iii) A bathochromic shift from 376 nm to 397 nm is associated to the electronic effects occurring when passing from vacuum to implicit solvation, to ONIOM QM/QM' and finally to SC-Ewald embedding (CAM-B3LYP). Such a trend goes towards the experimental transition of 471 nm

(though graphically, the λ_{max} is located even closer at ca. 440 nm); iv) the same magnitude of bathochromic shift is observed for B3LYP, going from 452 nm to 468 nm.

In the following, it will be shown that the enhanced emission observed upon aggregation of DPF can be rationalized considering only a single molecule, with the condition that one must account for the influence of the solid state environment. **Figure 4** shows the calculated and experimental emission spectra. Experimentally, it is observed that concentrated solutions of DPF dissolved in tetrahydrofuran produce two distinct emission bands. The first band, at 360 nm (3.44 eV), is attributed to emission from isolated molecules of DPF in solution (E_{SOL}) whereas the second band, at 534 nm (2.32 eV), is attributed to emission from the DPF aggregate (E_{AGG}). Importantly, E_{AGG} is not observed in low concentration (20 μM) THF solutions of DPF, due to the absence of aggregate formation.[16] In the following, we approximate the aggregated form of DPF as a perfect crystal. Due to the near-identical emission behavior observed experimentally for powdered and aggregated DPF and the precipitate-like nature of the aggregate, we deem this approximation to be viable.

From calculations performed on a single molecule of DPF, both in THF solution and by approximating the crystalline environment, E_{SOL} can be attributed to radiative emission from the S_3 state, which corresponds to a π-π^* excited state (**Figure 3**). From Figure 4 it can be seen that, of all of the models tested E_{SOL} is best reproduced, albeit with a marginal blue shift, using the THF solvent model which results in a calculated emission energy approximately 0.2 eV from the experimental value. The solid-state models, however, yield a significantly blue shifted (by 0.5 eV) emission maximum relative to experiment. Given the superior performance of the THF model, these results support that E_{SOL} is indeed a result of emission from isolated monomers of DPF in solution. Additionally, it can be seen that both solid state models – ONIOM QM/QM' and SC-Ewald – produce similar emission bands. This is significant, as it is an indication that the

close-range electrostatic interactions are well reproduced by the SC-Ewald approach, despite relying on simple point charges to approximate the crystalline environment. Furthermore, although SC-Ewald approximates the excited state crystalline potential while ONIOM approximates the ground state environment, due to the small spatial difference in density between the ground state and S_3 excited state it is to be expected that the ground and excited state potentials – and thus the resulting emission energies – will be similar.

Now considering E_{AGG} – a result of emission from the S_1 CT excited state ($S_1 \rightarrow S_0$) – all models produce emission energies comparable with experiment, with errors of just 0.11, 0.12 and 0.05 eV for THF, ONIOM and SC-Ewald, respectively. In contrast to E_{SOL}, ONIOM and SC-Ewald yield somewhat different emission energies for E_{AGG}, with SC-Ewald producing an emission energy that is 0.15 eV red-shifted with respect to ONIOM. Again, this is significant and highlights the state-specific nature of the excited state crystalline potential generated by SC-Ewald. Naturally, the pronounced charge transfer character of the S_1 excited state results in a marked rearrangement of the electronic density and, consequently, a non-negligible alteration to the surrounding embedding potential, which is reflected in the calculated emission energy.

Perhaps more interesting within the context of AIE is the difference in relative intensity between E_{SOL} and E_{AGG} produced by each model. In the case of THF, the weak emission from the S_1 state relative to that of the S_3 state is consistent with the lack of emission intensity observed experimentally for DPF in THF solution. Upon introducing the solid-state environment via the ONIOM model, a marginal enhancement of E_{AGG} can be noticed, in terms of brightness, although this is not of a sufficient magnitude to account for the experimentally measured enhanced emission of the aggregate. However, when accounting for the excited state crystalline potential as produced by SC-Ewald, a remarkable agreement with the experimental spectrum is observed, and the enhanced emission as a result of the aggregation is recovered. In this way, the potentially

non-negligible effects of not only the long-range electrostatic interactions but also the excited solid state potential are evident. Crucially, using this model it can be shown that both the large red-shift and enhanced emission intensity upon aggregation of DPF can be rationalized with a single molecule, without considering intermolecular electronically excited states or excimer formation. Notably, this is in contrast to the previous experimental interpretation, which relies on the formation of so-called "static excimers" – comprising dimers of DPF – to account for the 150 nm red-shift upon aggregation.

4. Conclusions

Our results demonstrate how, generally, modelling different environmental effects to a sufficient quality is crucial for the understanding and reproduction of experimental observations within the context of AIE. More specifically, in the case of DPF, it has been shown that the often-cited restriction of intramolecular rotation paradigm provides an incomplete picture of the AIE process in this particular case. Instead, a theoretical analysis has shown that the concomitant red-shift and fluorescence-enhancement upon aggregation of DPF monomers in solution is due to an environmentally driven process, relying on both short- and long-range excited state electrostatic interactions between a single molecule and its surroundings within the aggregate. We therefore suggest that the excited-state field of the environment enables the enhanced emission of otherwise poorly emissive, low-lying excited states and leads to an observed intense aggregate emission at lower wavelength with respect to solution. Interestingly, this lies in contrast to the previous interpretation of experimental results, which cite the formation of so-called "static excimers". We envisage that, for other reported cases of AIE accompanied by a significant changes in emission maxima, this protocol could be generally applied as a tool not only to understand, but to aid in the design of better-performing materials by providing a means of accommodating interaction with complex environments.

Supporting Information. Molecular scheme and crystalline structure of DPF, main structural parameters, structure of the two dimers' clusters and their calculated UV-Vis. absorption spectra, Complete References 10, 24, 25

Acknowledgements

DP and LW contributed equally to this work. Computational resources for this work were granted by the 'Projet 100339' (2015) at GENCI-IDRIS (Orsay, France).

References

(1) Birks, J. B. *Photophysics of Aromatic Molecules*; Wiley-Interscience: London, 1970.

(2) El′tsov, A. *Organic Photochromes*, Plenum.; New York, 1990.

(3) Crano, J. C.; Guglielmetti, R. J. *Organic Photochromic and Thermochromic Compounds*; Topics in Applied Chemistry; Plenum Press: New York, 1999.

(4) Tang, C. W.; VanSlyke, S. A. Organic Electroluminescent Diodes. *Appl. Phys. Lett.* **1987**, *51*, 913–915.

(5) Zhao, Z.; Chen, S.; Deng, C.; Lam, J. W. Y.; Chan, C. Y. K.; Lu, P.; Wang, Z.; Hu, B.; Chen, X.; Lu, P.; et al. Construction of Efficient Solid Emitters with Conventional and AIE Luminogens for Blue Organic Light-Emitting Diodes. *J. Mater. Chem.* **2011**, *21*, 10949–10956.

(6) Ding, D.; Li, K.; Liu, B.; Tang, B. Z. Bioprobes Based on AIE Fluorogens. *Acc. Chem. Res.* **2013**, *46*, 2441–2453.

(7) Mei, J.; Leung, N. L. C.; Kwok, R. T. K.; Lam, J. W. Y.; Tang, B. Z. Aggregation-Induced Emission: Together We Shine, United We Soar! *Chem. Rev.* **2015**, *115*, 11718–11940.

(8) Shustova, N. B.; Ong, T.-C.; Cozzolino, A. F.; Michaelis, V. K.; Griffin, R. G.; Dincă, M. Phenyl Ring Dynamics in a Tetraphenylethylene-Bridged Metal–Organic Framework: Implications for the Mechanism of Aggregation-Induced Emission. *J. Am. Chem. Soc.* **2012**, *134*, 15061–15070.

(9) Kasha, M. Energy Transfer Mechanisms and the Molecular Exciton Model for Molecular Aggregates. *Radiat. Res.* **1963**, *20*, 55–70.

(10) Luo, J.; Xie, Z.; Lam, J. W. Y.; Cheng, L.; Chen, H.; Qiu, C.; Kwok, H. S.; Zhan, X.; Liu, Y.; Zhu, D.; et al. Aggregation-Induced Emission of 1-Methyl-1,2,3,4,5-Pentaphenylsilole. *Chem. Commun.* **2001**, No. 18, 1740–1741.

(11) Zhao, Z.; He, B.; Tang, B. Z. Aggregation-Induced Emission of Siloles. *Chem. Sci.* **2015**, *6*, 5347–5365.

(12) Padalkar, V. S.; Seki, S. Excited-State Intramolecular Proton-Transfer (ESIPT)-Inspired Solid State Emitters. *Chem. Soc. Rev.* **2015**, *45*, 169–202.

(13) Wu, Q.; Deng, C.; Peng, Q.; Niu, Y.; Shuai, Z. Quantum Chemical Insights into the Aggregation Induced Emission Phenomena: A QM/MM Study for Pyrazine Derivatives. *J. Comput. Chem.* **2012**, *33*, 1862–1869.

(14) Wu, Q.; Peng, Q.; Niu, Y.; Gao, X.; Shuai, Z. Theoretical Insights into the Aggregation-Induced Emission by Hydrogen Bonding: A QM/MM Study. *J. Phys. Chem. A* **2012**, *116*, 3881–3888.

(15) Li, Z.; Dong, Y. Q.; Lam, J. W. Y.; Sun, J.; Qin, A.; Häußler, M.; Dong, Y. P.; Sung, H. H. Y.; Williams, I. D.; Kwok, H. S.; et al. Functionalized Siloles: Versatile Synthesis, Aggregation-Induced Emission, and Sensory and Device Applications. *Adv. Funct. Mater.* **2009**, *19*, 905–917.

(16) Yuan, M.-S.; Wang, D.-E.; Xue, P.; Wang, W.; Wang, J.-C.; Tu, Q.; Liu, Z.; Liu, Y.; Zhang, Y.; Wang, J. Fluorenone Organic Crystals: Two-Color Luminescence Switching and Reversible Phase Transformations between Π–π Stacking-Directed Packing and Hydrogen Bond-Directed Packing. *Chem. Mater.* **2014**, *26*, 2467–2477.

(17) Yuan, M.-S.; Du, X.; Xu, F.; Wang, D.-E.; Wang, W.-J.; Li, T.-B.; Tu, Q.; Zhang, Y.; Du, Z.; Wang, J. Aggregation-Induced Bathochromic Fluorescent Enhancement for Fluorenone Dyes. *Dyes Pigments* **2015**, *123*, 355–362.

(18) Xu, F.; Wang, H.; Du, X.; Wang, W.; Wang, D.-E.; Chen, S.; Han, X.; Li, N.; Yuan, M.-S.; Wang, J. Structure, Property and Mechanism Study of Fluorenone-Based AIE Dyes. *Dyes Pigments* **2016**, *129*, 121–128.

(19) Wilbraham, L.; Adamo, C.; Labat, F.; Ciofini, I. Electrostatic Embedding To Model the Impact of Environment on Photophysical Properties of Molecular Crystals: A Self-Consistent Charge Adjustment Procedure. *J. Chem. Theory Comput.* **2016**, *12*, 3316–3324.

(20) Corni, S.; Cammi, R.; Mennucci, B.; Tomasi, J. Electronic Excitation Energies of Molecules in Solution within Continuum Solvation Models: Investigating the Discrepancy between State-Specific and Linear-Response Methods. *J. Chem. Phys.* **2005**, *123*, 134512.

(21) Becke, A. D. Density□functional Thermochemistry. III. The Role of Exact Exchange. *J. Chem. Phys.* **1993**, *98*, 5648–5652.

(22) Lee, C.; Yang, W.; Parr, R. Development of the Colle-Salvetti Correlation-Energy Formula into a Functional of the Electron-Density. *Phys. Rev. B* **1988**, *37*, 785–789.

(23) Yanai, T.; Tew, D. P.; Handy, N. C. A New Hybrid Exchange–correlation Functional Using the Coulomb-Attenuating Method (CAM-B3LYP). *Chem. Phys. Lett.* **2004**, *393*, 51–57.

(24) Frisch, M. J.; Trucks, G. W.; Schlegel, H. B.; Scuseria, G. E.; Robb, M. A.; Cheeseman, J. R.; Scalmani, G.; Barone, V.; Petersson, G. A.; Nakatsuji, H.; et al. *Gaussian 09 Revision D.01*; Wallingford CT, 2009.

(25) R. Dovesi; V. R. Saunders; C. Roetti; R. Orlando; C. M. Zicovich-Wilson; F. Pascale; K. Doll; N. M. Harrison; B. Civalleri; I. J. Bush; et al. *CRYSTAL09 User's Manual*; Università di Torino: Torino, 2010.

(26) Dovesi, R.; Orlando, R.; Civalleri, B.; Roetti, C.; Saunders, V. R.; Zicovich-Wilson, C. M. CRYSTAL: A Computational Tool for the Ab Initio Study of the Electronic Properties of Crystals. *Z. Krist.* **2005**, *220*, 571–573.

(27) Civalleri, B.; Zicovich-Wilson, C. M.; Valenzano, L.; Ugliengo, P. B3LYP Augmented with an Empirical Dispersion Term (B3LYP-D*) as Applied to Molecular Crystals. *Crystengcomm* **2008**, *10*, 405–410.

(28) Presti, D.; Labat, F.; Pedone, A.; Frisch, M. J.; Hratchian, H. P.; Ciofini, I.; Menziani, M. C.; Adamo, C. Computational Protocol for Modeling Thermochromic Molecular Crystals: Salicylidene Aniline As a Case Study. *J. Chem. Theory Comput.* **2014**, *10*, 5577–5585.

(29) Presti, D.; Labat, F.; Pedone, A.; Frisch, M. J.; Hratchian, H. P.; Ciofini, I.; Cristina Menziani, M.; Adamo, C. Modeling Emission Features of Salicylidene Aniline Molecular Crystals: A QM/QM' Approach. *J. Comput. Chem.* **2016**, *37*, 861–870.

(30) Presti, D.; Pedone, A.; Ciofini, I.; Labat, F.; Menziani, M. C.; Adamo, C. Optical Properties of the Dibenzothiazolylphenol Molecular Crystals through ONIOM Calculations: The Effect of the Electrostatic Embedding Scheme. *Theor. Chem. Acc.* **2016**, *135*, 1–11.

(31) Klintenberg, M.; Derenzo, S. E.; Weber, M. J. Accurate Crystal Fields for Embedded Cluster Calculations. *Comput. Phys. Commun.* **2000**, *131*, 120–128.

(32) Weber, J.; Günne, J. S. auf der. Calculation of NMR Parameters in Ionic Solids by an Improved Self-Consistent Embedded Cluster Method. *Phys. Chem. Chem. Phys.* **2009**, *12*, 583–603.

(33) Bloino, J.; Biczysko, M.; Santoro, F.; Barone, V. General Approach to Compute Vibrationally Resolved One-Photon Electronic Spectra. *J. Chem. Theory Comput.* **2010**, *6*, 1256–1274.

(34) Baiardi, A.; Bloino, J.; Barone, V. General Time Dependent Approach to Vibronic Spectroscopy Including Franck–Condon, Herzberg–Teller, and Duschinsky Effects. *J. Chem. Theory Comput.* **2013**, *9*, 4097–4115.

(35) Jacquemin, D.; Brémond, E.; Planchat, A.; Ciofini, I.; Adamo, C. TD-DFT Vibronic Couplings in Anthraquinones: From Basis Set and Functional Benchmarks to Applications for Industrial Dyes. *J. Chem. Theory Comput.* **2011**, *7*, 1882–1892.

(36) Jacquemin, D.; Brémond, E.; Ciofini, I.; Adamo, C. Impact of Vibronic Couplings on Perceived Colors: Two Anthraquinones as a Working Example. *J. Phys. Chem. Lett.* **2012**, *3*, 468–471.

(37) Muniz-Miranda, F.; Pedone, A.; Battistelli, G.; Montalti, M.; Bloino, J.; Barone, V. Benchmarking TD-DFT against Vibrationally Resolved Absorption Spectra at Room Temperature: 7-Aminocoumarins as Test Cases. *J. Chem. Theory Comput.* **2015**, *11*, 5371–5384.

(38) Dreuw, A.; Weisman, J. L.; Head-Gordon, M. Long-Range Charge-Transfer Excited States in Time-Dependent Density Functional Theory Require Non-Local Exchange. *J. Chem. Phys.* **2003**, *119*, 2943–2946.

Figure 1. Schematic representation of the solid state models used in this work. (a) Solid state modeled using a two-level ONIOM QM/QM' scheme, with the low-level region including 20 nearest-neighbor molecules. (b) Solid state modeled using the ground (absorption) or excited state (emission) potentials generated by the SC-Ewald procedure, outlined in Ref.[19] Fitted charges (grey cube, Zone 3) are used to reproduce the excited state infinite crystalline potential within a given zone (red ball, Zone 2). Within this zone, a quantum-mechanically treated cluster is placed (black molecule, Zone 1).

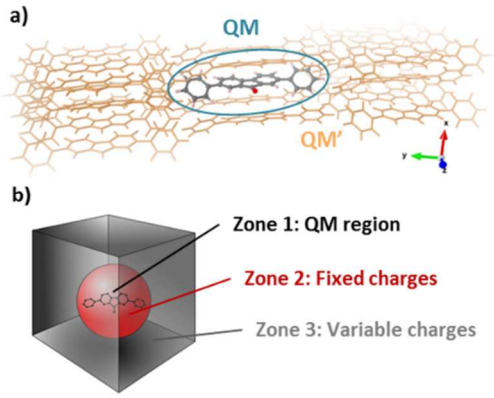

Figure 2. (a) Absorption spectra of dimer clusters extracted from the crystalline structure of DPF, computed at the CAM-B3LYP level of theory for two different dimer configurations: **Dimer 1** (b) and **Dimer 2** (c). These spectra have been obtained both in vacuum (solid lines) and using the ONIOM QM/QM' cluster model (dotted lines). A FWHM value of 0.35 eV is used throughout. For comparison, analogous calculations performed on monomers and the experimental spectrum[16] are given.

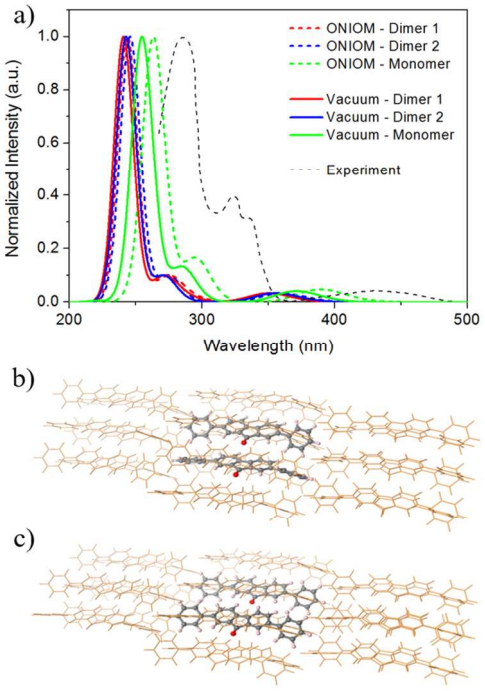

Figure 3. Calculated absorption spectra of DPF at the (a) B3LYP and (b) CAM-B3LYP level, adopting four different models to approximate the environment: i) in vacuum, ii) in THF, using implicit solvation, iii) in the solid state using an ONIOM QM/QM' model and iv) in the solid state using the ground state embedding potential as determined by the SC-Ewald procedure. A FWHM value of 0.35 eV is used throughout. The experimental absorption spectrum[16] is also shown (dashed lines). (c) Assignment and molecular orbitals involved in first three bright transitions ($S_1 \leftarrow S_0$, $S_3 \leftarrow S_0$, and $S_5 \leftarrow S_0$) of DPF (orbital isocontour value of 0.03 a.u.) along with the experimental absorption energies of the relevant bands.

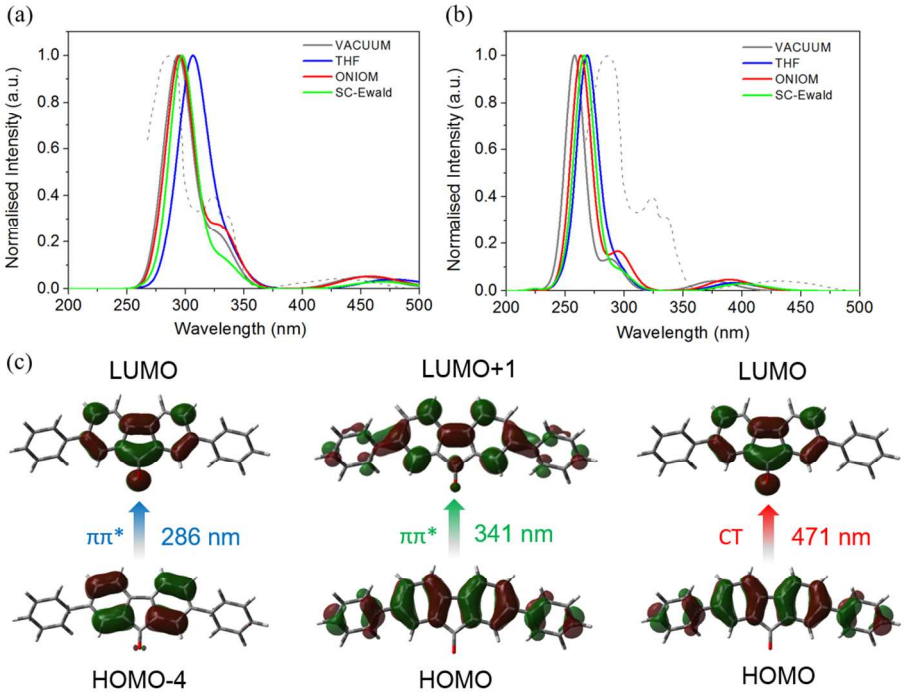

Figure 4. Calculated emission spectra of both $S_1 \rightarrow S_0$ and $S_3 \rightarrow S_0$ transitions at the CAM-B3LYP level: i) in THF (implicit solvation, C-PCM), ii) in the solid state using ONIOM QM/QM' and iii) in the solid state using the SC-Ewald embedding procedure. A FWHM value of 0.35 eV is used throughout. The experimental spectrum is also shown (dashed lines). E_{SOL} and E_{AGG} indicate experimental emission bands attributed to dissolved and aggregated DPF respectively. All spectra are normalized with respect to E_{AGG}.

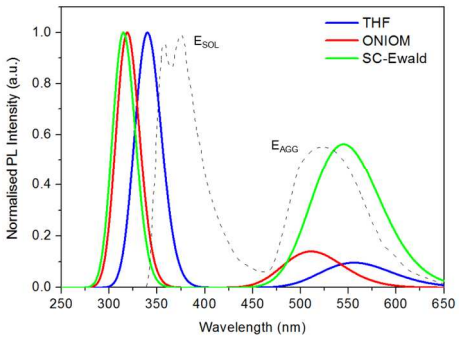

TOC GRAPHICS